Journal of Marine Science and Technology

Volume 28 | Issue 5 Article 11

ROBOTIC SUTURING IN MINIMALLY INVASIVE SURGERY

Jia-Yush Yen
Department of Mechanical Engineering, National Taiwan University, Taipei, Taiwan.

Hao-Xiang Kang
Department of Electrical Engineering, National Taiwan University, Taipei, Taiwan, aasdfghjkl129574ytw@gmail.com

Kuan Shen
Department of Electrical Engineering, National Taiwan University, Taipei, Taiwan

Yung-Yaw Chen
Department of Surgery, College of Medicine, National Taiwan University Hospital. Taipei, Taiwan

Ming-Chih Ho
Department of Surgery, College of Medicine, National Taiwan University Hospital. Taipei, Taiwan

ROBOTIC SUTURING IN MINIMALLY INVASIVE SURGERY

Acknowledgements

This work was supported in part by the Ministry of Science and Technology under Grant MOST 107-2221-E-002-177- MY3.

Journal of Marine Science and Technology, Vol. 28, No. 5, pp. 411-421 (2020)
DOI: 10.6119/JMST.202010_28(5).0011

ROBOTIC SUTURING IN MINIMALLY INVASIVE SURGERY

Jia-Yush Yen [1], Hao-Xiang Kang [2], Kuan Shen [2], Yung-Yaw Chen [3], and Ming-Chih Ho [3]

Key words: minimally invasive surgery, MIS robot, remote center of motion, surgical suturing.

ABSTRACT

Minimally invasive surgery (MIS) has the advantages of minimal bleeding and rapid postoperative recovery, which can alleviate patient suffering. Therefore, MIS is widely used in clinical applications. However, MIS is more difficult than traditional surgery; surgeons must be more meticulous when performing MIS than when performing ordinary surgery. Using a robotic arm in an auxiliary role in MIS can reduce the workload of surgeons and increase the precision and efficiency of the surgical procedure. The aim of this article is to design an MIS robot system that can perform automatic surgical suturing. First, we designed the basic control architecture for a remote-control-of-motion MIS robot with eight degrees of freedom. The surgical instrument was operated in the abdominal cavity without causing lacerations to the patient's abdomen. The surgical suture motion was then performed using the robot arm in the abdominal cavity. The correctness of the control algorithm and the surgical suture motion was verified through simulation. Finally, the feasibility of using an MIS robot for surgical suturing was verified through experiments.

I. INTRODUCTION

Traditional hepatic resection involves removing livers through laparotomy. In conventional surgery using cutting instruments, a surgeon makes a lateral chevron incision that is 15 cm or more along the lower edge of the rib on the abdomen of the patient (Patnaik, 2011). However, this method causes visceral exposure of a large area, which increases the risk of infection. Moreover, large incisions increase the postoperative recovery time. Many patients experience pain after such surgeries. Daily activities such as walking, eating, and even breathing are affected. Large incisions can result in seriously ill patients having problems such as adhesion ileus and hernia. By contrast, MIS only requires small incisions on the patient's abdomen and causes less laceration during surgery. The incisions can be as small as 15 mm (M. Berducci, 2016). Thus, blood loss is limited and postoperative recovery time is reduced. Typically, in a traditional surgery, 500 g of blood is lost. In a MIS, blood loss is restricted to 300 g. Furthermore, in MIS, the three-year survival rate can be increased from 70% to 95% and the relapse rate decreases from 36% to 8%. The recovery time considerably decreases from around 20 days to 10 days. Furthermore, disputes after surgery have been minimized from 50% to 13% (Laurent et al., 2003; Kanekos et al., 2005; Belli et al., 2009; Tranchart et al., 2010). Because of these advantages, MIS is the best option for substituting traditional hepatic resection. With the enhancement of MIS techniques and machines, many traditional hepatic resections, including gall bladder, liver, and kidney, can be replaced by MIS laparoscopy. MIS benefits many patients and reduces medical costs.

When doctors perform surgeries, their energy and accuracy decrease with the increase in the operating time. To minimize surgeon effort during surgeries, this study simulated the suturing motion in MIS using an eight-degree-of-freedom integrated driving system.

The purpose of this paper is to provide solutions for the aforementioned problems associated with conventional surgery. The target is to automate the suturing process in MIS and increase stability and efficiency. To achieve this, an MIS robot with a high degree of freedom can be used to perform suturing motions in MIS. This can alleviate surgeon strain during surgery and increase precision and efficiency.

The mechanical design can be separated into two parts, namely the mechanisms being placed inside and outside the abdomen. The mechanism outside drives the endoscopic instrument exactly in the manner surgeons operate. The mechanism should be sufficiently flexible enough to complete the suturing tasks. In the mechanism placed inside the abdomen,

Paper submitted 01/08/20; revised 05/11/20; accepted 07/06/20. Corresponding Author: Hao-Xiang Kang (e-mail:aasdfghjkl129574ytw@gmail.com)
[1]Department of Mechanical Engineering, National Taiwan University, Taipei, Taiwan.
[2]Department of Electrical Engineering, National Taiwan University, Taipei, Taiwan.
[3]Department of Surgery, College of Medicine, National Taiwan University Hospital. Taipei, Taiwan

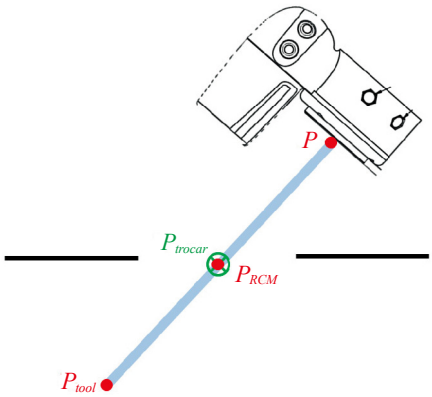

Fig. 1. The schematic diagram of the l EndoWrist in MIS

a needle is clamped with a special apparatus. The mechanism placed outside the abdomen is used to move the needle to complete the suturing motion precisely. To satisfy the aforementioned requirements, the da Vinci EndoWrist instrument with two degrees of freedom was combined with a robotic arm with six degrees of freedom to obtain an integrated driving system with eight degrees of freedom. As a result, multiple degrees of freedom and wide joint range ensured that the wrist and the clamp of the end effector could perform multiple and complex motions.

For the controlling part, when the EndoWrist instrument is inserted into the abdomen, the trocar point should be fixed to avoid injury to patients. Thus, when controlling the robotic arm to operate the surgery mechanism, in addition to the previous conditions, the motion of the end effector must follow the desired trajectory. The desired surgery motion can be completed by adjusting the configuration of the mechanism placed inside the abdomen. After the basic controlling system had been designed, the suturing motion of MIS was analyzed. The purpose is to plan suitable motion commands and ensure the surgery robot can complete suturing tasks. This can automate the suturing process in MIS and prove the feasibility of the surgery robot system proposed in this paper.

II. THEORY ANALYSIS

1. Controller design of RCM

The long tube fixed on the robotic arm should not cause lacerations in the abdomen during end-effector movements. When one controls the movement of the end effector, the constraints of the remote center-of-motion (RCM) must be considered. There're two constraints on the intersection of the long tube and the imagined plane of the abdomen because of the control positions of end- effector and the intersection.

The schematic of the EndoWrist fixed on the robotic arm after insertion into the patient's abdomen is depicted in Fig.1.

Here, P is the end of the sixth axis of the robotic arm and P_{tool} is the end of the extending long tube, which is the same as the location of the surgery mechanism. Furthermore, P_{trocar} is the center of the incision on the abdomen, which is a fixed point relative to base coordinates. In the diagram, P_{RCM} is a point on the long tube that is closest to P_{trocar} and changes relative to robot coordinates. To describe P_{RCM} more conveniently, we define the parameter λ, which refers to the proportion of the long tube outside the abdomen. The definition is expressed as follows:

$$\lambda = \frac{|P_{trocar} - P|}{L_{tube}} \tag{1}$$

The numerator refers to the distance between P_{trocar} and P. Here, L_{tube} refers to the length of the tube between P and P_{tool}. After λ has been specified, P_{RCM} can be described as follows:

$$P_{RCM} = P + \lambda(P_{tool} - P) \tag{2}$$

When P_{tool} is moving in the abdomen, the location of P_{RCM} must be fixed at P_{trocar}. The transformational relationship between P_{RCM} and the joint angular velocity of the robotic arm is expressed as follow:

$$\dot{P}_{RCM_{3\times1}} = J_{RCM\ 3\times6}\,\dot{q}_{6\times1} \tag{3}$$

To satisfy these requirements, a suitable controller for the robotic arm was designed for the model of the robotic arm. The controller has two requirements: the first is to provide the path for the end effector to move along in the Cartesian space; the second is the limited condition of the RCM. We define the following errors:

$$e_{tool} = P_{tool\_d} - P_{tool} \tag{4}$$

$$e_{RCM} = P_{trocar} - P_{RCM} \tag{5}$$

Given the differential equations of P_{RCM} and P_{tool}, the two kinematics equation systems can be combined to form a new kinematic controlling system. Therefore, we define the following expression:

$$J = \begin{vmatrix} J_{tool} \\ J_{RCM} \end{vmatrix} \tag{6}$$

J_{tool} and J_{RCM} are the Jacobian of the P_{tool} and P_{RCM} when the suturing is operating. We apply the inverse Jacobian method to design the joint angular velocity as follows:

$$\dot{q} = J^{+} \begin{vmatrix} k_1 e_{tool} \\ k_2 e_{RCM} \end{vmatrix} \tag{7}$$

J^{+} is the pseudoinverse of J in (6). For the path control and the control of RCM, gains k_1 and k_2, respectively, can be designed.

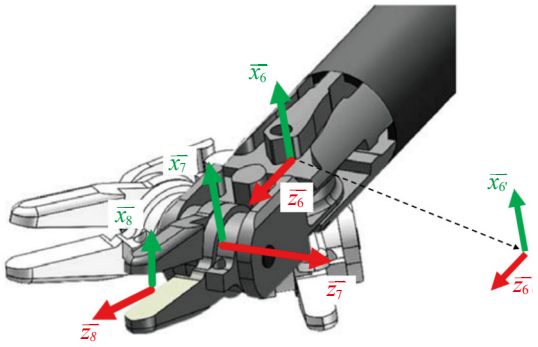

Fig. 2. EndoWrist coordinates

2. Kinematics model of the EndoWrist instrument

The end-effector movement in space was controlled as previously mentioned. Then, a two-degree-of-freedom mechanism, composed of a wrist and clamp, was added at the end of the long tube. The expected configuration of the EndoWrist can be realized by adjusting the rotation angle of the mechanism. The relationship between the three rotation angles and the EndoWrist's configuration was analyzed using kinematics. To simplify the procedures, we defined the coordinate {6'} which was the location of the end of long tube when $\theta_6 = 0$. Then, the coordinates {6}, {7}, {8} were defined as follows:

θ_6、θ_7、θ_8 are the joint angles of the three coordinate refering to the Fig.2. The transformation matrix between {6'} and {6} is determined by the rotational angle θ_6 on the robotic arm, defined in the rotation matrix as follows:

$$ {}^{6}_{6'}R = \begin{bmatrix} c\theta_6 & -s\theta_6 & 0 \\ s\theta_6 & c\theta_6 & 0 \\ 0 & 0 & 1 \end{bmatrix} \tag{8} $$

The transformation matrix between {6} to {8}:

$$ {}^{7}_{6}R = \begin{bmatrix} 1 & 0 & 0 \\ 0 & c(\alpha_7 - \theta_7) & -s(\alpha_7 - \theta_7) \\ 0 & s(\alpha_7 - \theta_7) & c(\alpha_7 - \theta_7) \end{bmatrix} \tag{9} $$

$$ {}^{8}_{7}R = \begin{bmatrix} c\theta_8 & -s\theta_8 & 0 \\ s\theta_8 & c\theta_8 & 0 \\ 0 & 0 & 1 \end{bmatrix} \begin{bmatrix} 1 & 0 & 0 \\ 0 & c\alpha_8 & -s\alpha_8 \\ 0 & s\alpha_8 & c\alpha_8 \end{bmatrix} \tag{10} $$

In the formula, $\alpha_7 = -\pi/2$、$\alpha_8 = \pi/2$. The rotational matrix between the end of the EndoWrist and the clamp can be obtained by multiplying the aforementioned three matrices:

$$ \begin{aligned} {}^{6}_{6'}R &= {}^{6}_{6'}R\,{}^{7}_{6}R\,{}^{8}_{7}R \\ &= \begin{bmatrix} c\theta_6 c\theta_8 + s\theta_6 s\theta_7 s\theta_8 & -s\theta_6 c\theta_7 & c\theta_6 s\theta_8 + s\theta_6 s\theta_7 c\theta_8 \\ s\theta_6 c\theta_8 + c\theta_6 s\theta_7 s\theta_8 & c\theta_6 c\theta_7 & s\theta_6 s\theta_8 + c\theta_6 s\theta_7 c\theta_8 \\ -c\theta_7 s\theta_8 & -s\theta_7 & c\theta_7 c\theta_8 \end{bmatrix} \end{aligned} \tag{11} $$

${}^{6}_{6'}R$、${}^{7}_{6}R$、${}^{8}_{7}R$ are the rotation matrices between three coordinated mentioned in Fig.2. The orientation of the clamp can be determined by deriving the forward kinematics with three rotation angles. However, when adjusting the clamp to the desired configuration, the value of the three rotation angles can be calculated using inverse kinematics. Therefore, the expected configuration can be achieved for the clamp.

III. CONTROL LAW OF THE SYSTEM

1. Robotic arm control

Dynamic equations play a vital role in robotics. These equations describe the influences of the joint torque and external forces on the dynamics of the robot arm. Regarding the derivation of the dynamic equations, the Newton–Euler and Lagrange methods are the commonly used. Particularly, the Newton–Euler method involves less calculation and is therefore more commonly used in real-time controls. The dynamics of the robot arm can be expressed using a second-order nonlinear dynamic equation under the joint coordinate. The equation is expressed as follows:

$$ D(q)\ddot{q} + C(q,\dot{q})\dot{q} + G(q) = \tau - \tau_e \tag{12} $$

After we obtain the dynamic equation of the robot arm, we can determine the influences of the joint torque and external forces on the dynamics of the robot arm. On the basis of the relevant equations, the inverse dynamic equation can be applied to a complex nonlinear control system. The linearization and decoupling of the dynamic equation can be achieved using nonlinear feedback control systems and appropriate control algorithms to track the trajectories of the joint angles. Regardless of the influences of external forces, we can modify (12) as follows:

$$ \tau = D(q)\ddot{q} + C(q,\dot{q})\dot{q} + G(q) \tag{13} $$

This dynamic equation is a nonlinear system and the design of the control law is more complex than linear systems. Based on the aforementioned concepts, the control law can be designed as follows:

$$ \tau = \alpha a_q + \beta \tag{14} $$

The purpose of β is to estimate the nonlinear terms of the dynamic systems. After the nonlinear terms have been removed, the controller can be designed under the conditions of linear systems. Thus, β can be designed as follows:

$$ \beta = C(q,\dot{q})\dot{q} + G(q) \tag{15} $$

To adjust the dynamics of the system, α is held equal to $D(q)$. Then $\ddot{q}$ can be defined as follows:

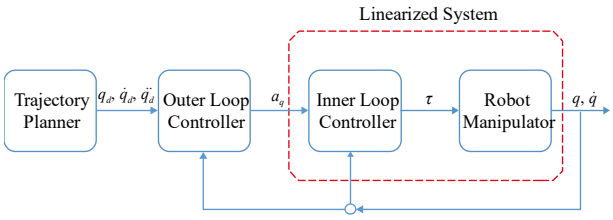

Fig. 3. Dynamic control law

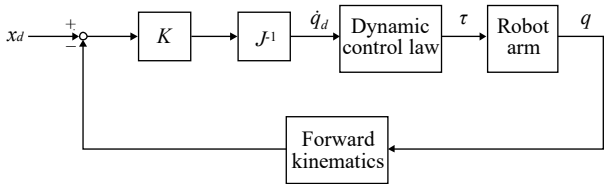

Fig. 4. The architecture of the inverse Jacobian

$$\ddot{q} = a_q \tag{16}$$

A double integrator system is described and is expressed as an double integrator of nth order decoupling. When the nonlinear terms have been removed using β, the system is linearized into a second-order linear decoupling system. Therefore, we only consider the design of a_q and the kth element of a_q, which only affects the dynamics of the k-axis. They do not influence each other. Based on the situation, a_q can be designed as follows:

$$a_q = \ddot{q}_d + K_d\dot{e} + K_p e \tag{17}$$

Here, e is the tracking error vector of the joint and q_d is the desired trajectory. K_d and K_p are the gains of the tracking error function. Therefore, the closed-loop dynamic response for the tracking error of joint can be defined as follows:

$$\ddot{e} + K_d\dot{e} + K_p e = 0 \tag{18}$$

By setting the gains K_d and K_p, the poles of the second-order system can be adjusted. When changing the dynamic response of the tracking error, each joint angle should match with the desired trajectory. Calculating the inertia matrix, Coriolis force, and the gravity matrix requires large and real-time calculation. A more convenient method is to separate the control law into inner and outer circuits and place the inner circuit into dedicated hardware interfaces such as digital signal processor for real-time calculation.

The system architecture is described below:

In the aforementioned architecture, a_q is the input and τ is the output of the inner circuit. The outer loop calculates the input command a_q. In addition, the design of the external feedback control system is simplified because the controlled body in the red dotted area can be regarded as a linear system. Therefore, the whole dynamic system can be calculated easily.

2. The controller of inverse Jacobian

It is difficult to intuitively determine the relationship between the end position of the robot arm and joint angle. Therefore, it is necessary to consider the conversion between the joint space and Cartesian space so that the robot arm can move according to the desired trajectory in the Cartesian space. The velocity conversion relationship between two coordinate systems can be expressed as follows:

$$\dot{x} = J(q)\dot{q} \tag{19}$$

Assuming that the robot arm's angular velocity command can be provided directly, the angular velocity command can be expressed as follows:

$$\dot{q}_d = J^{-1}K\left(x_d - x\right) \tag{20}$$

x_d and x represent the desired position command and the current end position of the robot arm, where x can be obtained from the joint angle. Here, K is the gain matrix and J^{-1} is the inverse of Jacobian matrix. In the case of non-square matrix of J, J^{+} can be used instead. After we obtain the joint angular velocity command of the robot arm, we can use the control law presented in Fig. 3 to convert the command of joint angular velocity into the corresponding reference torque command and drive the robot arm. The combined architecture of our inverse Jacobian and the control law is described in the following sections:

3. Damped least square method

Singularity problems are a concern when solving inverse kinematic problems. When a singularity occurs, the inverse of Jacobian matrix does not exist and adversely affects the motion of the robot arm. Therefore, we can use the damped least square method to avoid the scenario where the robot arm reaches the singularity points when designing the controller of inverse Jacobian. We can modify the pseudo-inverse matrix of Jacobian through the DLS method and minimize $\left(\left\|\dot{x} - J\dot{q}\right\|^2 + \sigma\left\|\dot{q}\right\|^2\right)$. The method can be defined as follows:

$$J_\sigma^+ = J^T(JJ^T + \sigma I_m)^{-1} \tag{21}$$

The damping factor σ can effectively avoid the occurrence of singularity points but it affects the evaluation of the joint angular velocity $\dot{q}$. Therefore, a range should be set for σ, which only functions near the singularity points and the value of the damping factor is zero at other points. The weighted value is defined as follows:

$$p(q) = \sqrt{\det(JJ^T)} \tag{22}$$

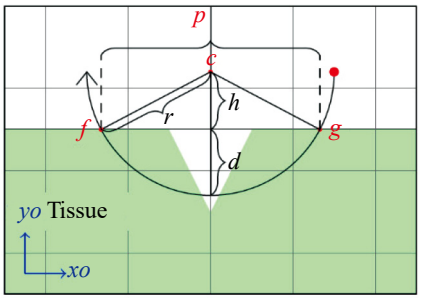

Fig. 5. Ideal path of suturing

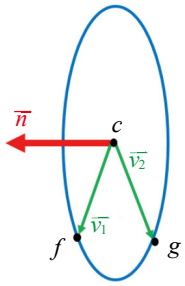

Fig. 6. Schematic of the path of suturing and the normal vector

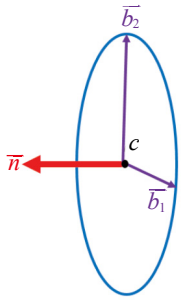

Fig. 7. Schematic of the vectors

The smaller the p value is, the closer it is to singularity. Based on this value, the damping factor should be adjusted as follows.

$$\sigma = \begin{cases} \sigma_0 \left(1 - \dfrac{p}{p^s}\right), if \;\; p < p^s \\ 0 \qquad\qquad ,otherwise \end{cases} \tag{23}$$

Here, p^s is a critical value near the singularity point and determines whether σ has an effect on the Jacobian and σ_0 is not only a value of the damping factor at the singular point but also the maximum value of the damping ratio. When the p value is less than p^s, the value of damping factor σ is not zero and this can avoid the occurrence of singularity points. By modifying the Jacobian matrix, σ will approach to the maximum value σ_0 when p is close to zero. By contrast, if the value p is greater than p^s, then the damping factor σ is zero and does not influence the Jacobian matrix. The aforementioned adjustments enable the robot arm to avoid the singularity point during the suturing process and avoid unnecessary impacts in the working space outside the singular points.

IV. TRJECTORY PLANNING FOR SUTURING

1. Ideal path for suturing

The ideal path of suturing is an arc with the same radius as the surgical suturing needle, that is, the path that can reduce the needle's resistance to the smallest extent during the suturing process (Fig. 5).

When planning the path of suturing, the aforementioned concept is used as the foundation. If the suturing needle is clamped by the surgery clamp and moves along the aforementioned arc, the moving path of the surgery clamp should be the same as that of the arc. A mathematical description of the arc should be determined first. The path of curve is hereafter described as the parametric equation.

We assumed that f and g, respectively, are the specific points the suturing needle enters and leaves tissue surfaces. c is the center of the suturing circle and d is the suturing depth refers to the tissue. h is the length between the center of the needle and the surface of the tissue. The circle of the ideal trajectory was in a plane perpendicular to the patient's abdomen. Furthermore, the radius of the suturing needle was fixed. With these three conditions, only a circle can be defined in the xy-plane. To describe this as the parametric equation, the position of the center of the circle in the plane should be determined beforehand. The geometric relationship in the figure can be used to determine the distance p between two points f and g as follows:

$$p = |f - g| \tag{24}$$

Because the length of f is fixed, the length of h refers to the distance between the center of circle and the surface of the tissue and can be determined from the following expression:

$$h = \sqrt{r^2 - \left(\frac{p}{2}\right)^2} \tag{25}$$

The center of the circle c can be defined as follows:

$$c = \frac{1}{2}(f + g) + h \begin{bmatrix} 0 \\ 0 \\ 1 \end{bmatrix} \tag{26}$$

Then, the expected path of suturing is determined. The normal vector of the surface is depicted in Fig. 6 as follows:

$\vec{v_1}$=f-c and $\vec{v_2}$=g-c. The normal vector is depicted as follows:

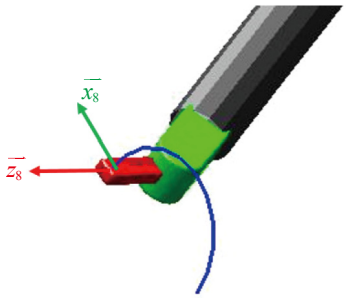

Fig. 8. Suturing clamp coordinate

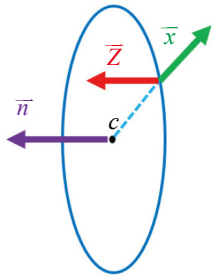

Fig. 9. Desirable suturing coordinate

$$\vec{n} = \frac{(\overrightarrow{v_2} \times \overrightarrow{v_1})}{\left|\overrightarrow{v_2} \times \overrightarrow{v_1}\right|} \tag{27}$$

Using the normal vector as the benchmark, the basis vectors of the planes $\overrightarrow{b_2}=[0 \quad 0 \quad 1]^T$ and $\overrightarrow{b_1}=\overrightarrow{b_2}\times\vec{n}$ are defined.

Using angle θ as a parameter and $\overrightarrow{b_1}$ and $\overrightarrow{b_2}$ as benchmarks, an arbitrary $\vec{r}$ can be described as follows:

$$\vec{r}(\theta) = r_{needle}\left(\overrightarrow{b_1}\cos\theta + \overrightarrow{b_2}\sin\theta\right) \tag{28}$$

The vector $\vec{r}$ represents the vector from the center of circle to any point on the path of suturing. Here, r_{needle} is the radius of the suturing needle. Using θ as the parameter when planning the moving path from the starting point to the ending point, $\Delta\theta$ can be defined as follows:

$$\Delta\theta = \left(\theta_f - \theta_i\right)/s \tag{29}$$

Where, θ_i and θ_f refer to the starting angle and the final angle of the motion planning, respectively, s represents the number of total inserted points in this path. Therefore, $\Delta\theta$ describes the difference of the angle between the two commanded points. Using the kth time step to describe $\vec{r}$, we obtain the following equation:

$$\vec{r}\left(k\right) = r_{needle}\left(\overrightarrow{b_1}\cos\left(\theta_i + k\Delta\theta\right) + \overrightarrow{b_2}\sin\left(\theta_i + k\Delta\theta\right)\right) \tag{30}$$

The commanded moving trajectory of the surgery clamp is depicted as follows:

$$P_{tool\_d}\left(k\right) = c + \vec{r}(k) \tag{31}$$

2. Solution of the acceptable angle

According to the coordinate definition of the surgery clamp, the relative position and direction of the surgery clamp and needle during the suturing process is depicted in Fig. 7.

If the surgery clamp and the curved path planned beforehand must be overlapped during the suturing process, then the direction of $\overrightarrow{z_8}$ must be fixed throughout the process. Thus, the directions of $\overrightarrow{z_8}$ and normal vector $\vec{n}$ of the curved path must be consistent. Furthermore, $\overrightarrow{x_8}$ should point outward to the circular arc, whereas $\overrightarrow{y_8}$ points to the tangential direction of the circular arc. According to the aforementioned requirements, the direction of the ideal configuration z-axis can be specified as $\vec{n}$. The x-axis is directed along the vector of the surgery clamp where the center of the circle points to. Therefore, the direction of the y-axis can be determined as follows:

$$\begin{cases} \overrightarrow{z_8} = \vec{n} \\ \overrightarrow{x_8} = \dfrac{(P_{tool\_d} - c)}{\left|P_{tool\_d} - c\right|} \\ \overrightarrow{y_8} = \overrightarrow{z_8} \times \overrightarrow{x_8} \end{cases} \tag{32}$$

As defined in the aforementioned coordinate, the desirable suturing coordinate can be defined according to Fig. 8. The suturing clamp coordinate should match the desirable suturing coordinate along with the arc path that is planned beforehand during the suturing process.

Based on the rotational relationship between the two coordinates, the column of the rotational matrix refers to the three-axis direction. This direction is the coordinate after transformation, which is based on the original coordinate. Therefore, (32) represents the rotational relationship between the ideal coordinate of the surgery clamp and benchmark coordinate of the robotic arm. The transformed rational matrix can be defined as follows:

$${}^{8}_{0}R_d = \begin{bmatrix} \overrightarrow{x_8} & \overrightarrow{y_8} & \overrightarrow{z_8} \end{bmatrix} \tag{33}$$

To determine θ_6, θ_7, and θ_8, the P_{tool_d} command can be sent to the integrated driving systems The corresponding θ_1 to θ_5 can then be solved using inverse kinematics and ignoring the lengths of link 7 and link 8 because of minor errors during the suturing process. The relationship between the rotational matrices of the last three coordinate axes can be defined as follows:

$${}^{8}_{6'}R_d = {}^{0}_{6'}R\ {}^{8}_{0}R_d = \left({}^{6}_{0'}R\right)^T {}^{8}_{0}R_d \tag{34}$$

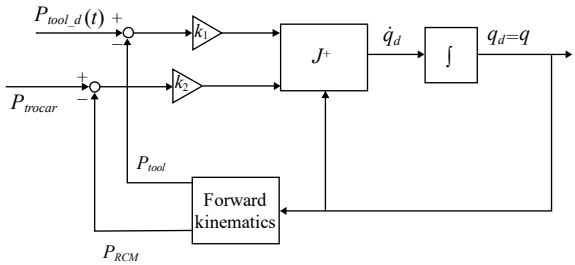

Fig. 10. Ideal Dynamic Control Law

We can solve (34) using (11) and θ_6、θ_7, and θ_8 can be solved using the following formula:

$$\begin{cases} \theta_6 = atan2\left(-{}^{8}_{6'}R_d(1,2), {}^{8}_{6'}R_d(2,2)\right) \\ \theta_8 = atan2\left(-{}^{8}_{6'}R_d(3,1), {}^{8}_{6'}R_d(3,3)\right) \\ \theta_7 = atan2\left({}^{8}_{6'}R_d(3,2)s\theta_8, {}^{8}_{6'}R_d(3,1)\right) \end{cases} \tag{35}$$

Eight solutions are obtained and the desirable solution should be unique. In addition to this answer, a wrong direction of the suturing clamp, which results in a wrong coordinate plane, is also obtained. Therefore, the error rotational matrix R_{error} is defined as follows:

$$R_{error} = {}^{8}_{6'}R(\theta_6, \theta_7, \theta_8) - {}^{8}_{6'}R_d \tag{36}$$

In theory, if the unique solution is found, the R_{error} calculated by the solution should be a zero matrix. However, the problem of the quantization error should be still considered. However, some minimal errors still occur. As a result, the minimal $\|R_{error}\|$ instead of the zero matrix should be determined.

3. Compensate trajectory error by recursive

To obtain values close to the real-world situations, the dynamics of the robotic arm are considered during the simulation. Therefore, the error maybe introduced from the joint angle tracking control. To verify the accuracy of the inverse kinematics control, it can be assumed that the dynamics of the robot arm attains the optimal state. Thus, no error is observed in the joint space during simulation. According to the methods mentioned above and the method in section III, the new control law can be derived with the following procedure.

The integrated driving system had eight degrees of freedom. We solved θ_1 to θ_8 by calculating inverse kinematics from the matrices obtained from θ_1 to θ_8. To simplifying this complex calculation, they can be separated into two parts. The first part is to solve θ_1 to θ_5 using inverse kinematics from the robot. Here, θ_1 to θ_5 controlled position of P_{tool}. In the second part, θ_6 to θ_8 were solved using previously mentioned algorithms. In contrast to the first part, the target of the second part is to match the suturing coordinate plane with the desirable suturing coordinate plane during the suturing process. However, the

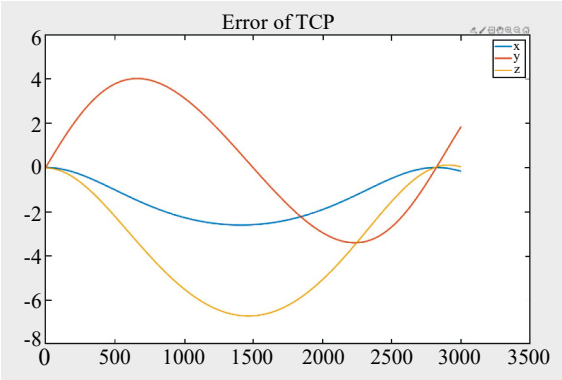

Fig. 11. Original trajectory error

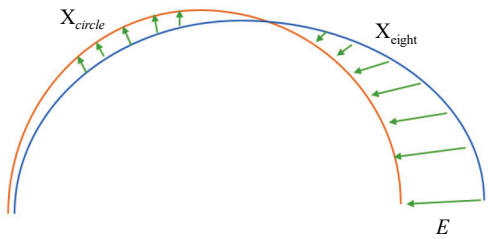

Fig. 12. Schematic of the recursive method

target that surgeons focus on is the endpoint of the needle instead of the end of the clamp. We cannot neglect the problem caused by deleting the lengths of link 7 and link 8. The trajectory error can then be computed as below.

Notice that the trajectory error was compensated by using the recursive method to adjust for the position of the needlepoint and minimizing the error.

The orange and blue curves denote the schematic line of the desirable motion of the needlepoint X_{cicle} and real motion of the needlepoint X_{eight}. Because the lengths of link 7 and link 8 were ignored, the trajectory error occurred. This is defined as follows:

$$e(1) = x_{cicle} - x_{eight}(1) \tag{37}$$

$e(1)$ refers to the first trajectory error. To correct the trajectory error formed by ignoring the lengths of link 7 and link 8, we repeated the process until the error converged to an acceptable value. The repeat process is depicted as follows:

$$\begin{aligned} x_{eight}(2) &= x_{circle} + e(1) \\ e(2) &= x_{cicle} - x_{eight}(2) \\ x_{eight}(3) &= x_{circle} + e(2) \\ e(3) &= x_{cicle} - x_{eight}(3) \\ x_{eight}(4) &= x_{circle} + e(3) \end{aligned} \tag{38}$$

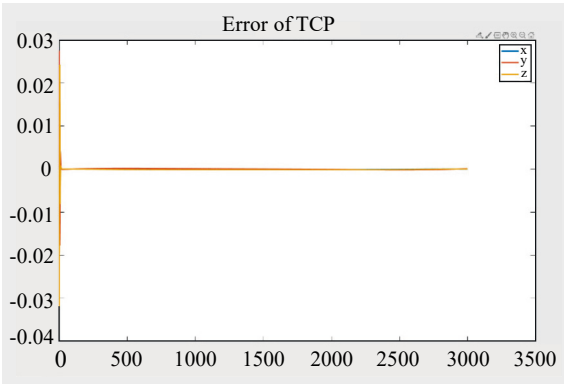

Fig. 13. Trajectory error after the fourth iteration of the trajectory correction

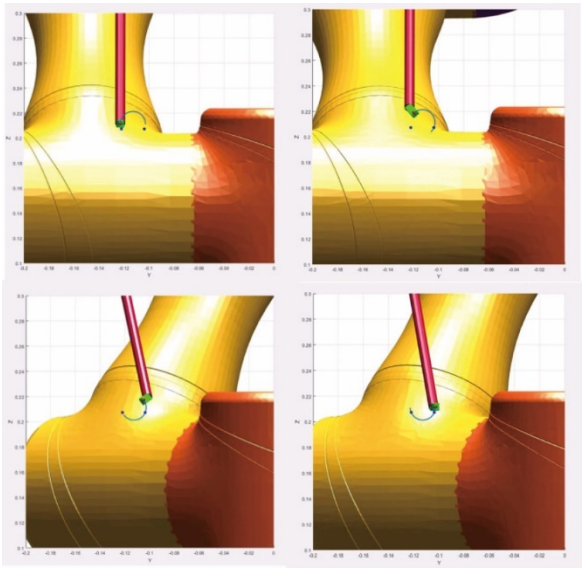

Fig. 14. Simulation of the suturing process

$e(2)$, $e(3)$ refer to the second and the third trajectory errors. $x_{eight}(2)$, $x_{eight}(3)$ refer to the first and the second revised needlepoint positions, and so on. Therefore, the trajectory error problems can be solved using the recursive method. The feasibility of the simplified method of separating the eight degrees of freedom into two parts is verified by the result.

Some fluctuations were observed at the beginning but the trajectory error converged quickly after the fluctuations. In conclusion, a minor trajectory error is not likely to affect the precision of the suturing process.

Because of the multiple degrees of freedom, the integrated driving system can perform the delicate motions of the surgery, which can ease the workload of surgeons.

V. STSTEM CONSTRUCTION

The robot arm used in this research was TM5-700. The robot arm satisfied the safety requirements of the collaborative

Fig. 15. TM robot (TM5-700)

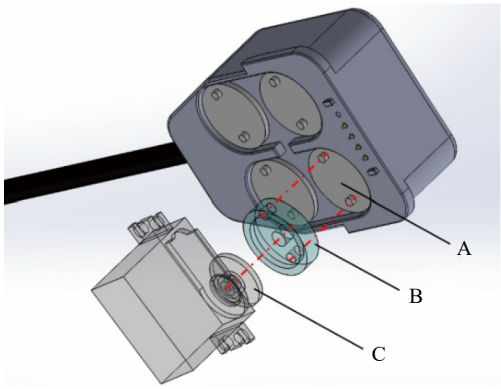

Fig. 16. Design of the connecting device

robot. When external collision is detected, the robot arm stops moving immediately to ensure the safety of the staffs. The electrical cabinet can communicate with RS232, Ethernet, and Modbus TCP/RTU. The TM robot can exchange information with the external devices.

The surgery clamp used in the experiment is the large needle driver of the da Vinci surgical system. This surgery clamp is an artificial arm that is driven using a wire. The major components of the clamp include the base, shell, shaft, mechanical wrist, and clamp. The diameter of the long tube shaft was 8 mm. The shaft can be placed into the patients' abdominal cavity to drive the movement of the front clamp by spinning the wheel on the base. The wire drives the mechanical wrist to rotate and change the direction of the clamp. The advantages of the drive-by-wire is that the end effector is more flexible and dexterous.

The design of the driving device is illustrated in Fig. 16. Two asymmetrical protrusions are present on the four wheels (A) of the base. The two holes on the designed wheels (B) can be used to match with the aforementioned protrusions. This can be fixed on the servomotor (C), which is the power source. The wheels in the basement can be rotated by rotating the motor and the wheels.

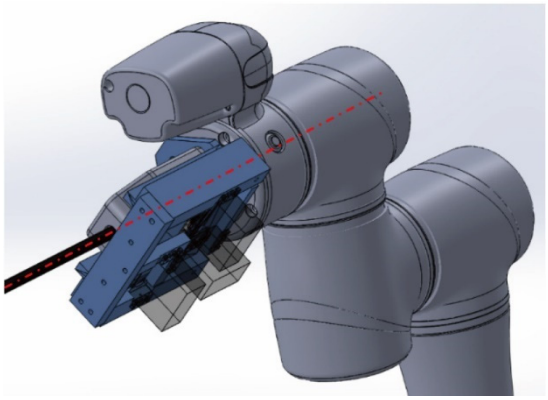

Fig. 17. Design of the integrated driving systems

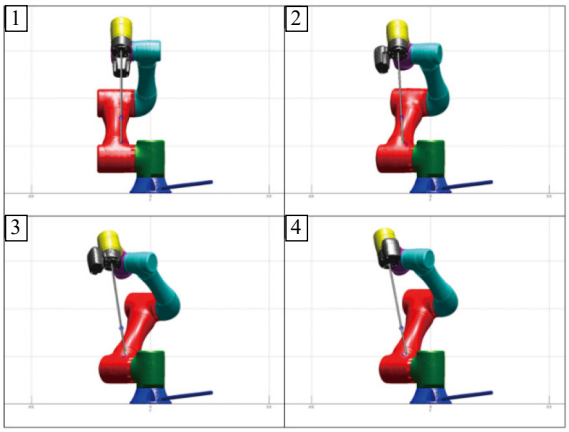

Fig. 18. Simulation of the movement of surgical suturing needle

The relative location between the servomotor and wheel in the base should be consistent when designing the fixed device. Fig. 16. depicts that the servomotors are mounted to the driving wheels using the homemade couplings. Moreover, the shaft of the surgery clamp should be coaxial with the sixth z-axis of the robotic arm after the surgery clamp is fixed on the fixing device and combined with the end of the robotic arm. If any bias occurs, the controlling accuracy of the RCM is affected.

VI. EXPERIMENTS

After the kinematics and dynamics parameters of the robotic arm had been processed with the RVC tool within MATLAB, our mathematical model of the arm was constructed. Simulation was used to test whether the controlling system satisfies the requirements. Various experiments are then carried out for validation.

The rotational command in the joint space is $[\theta_{1d} \quad \ldots \quad \theta_{8d}]^T$. The command consists of the eight joint rotational angles, with θ_{1d}~θ_{6d} as the commands for driving the back-end robot arm and θ_{7d}, θ_{8d} as the commands for driving the Endowrist instrument. The computer serves as the upper

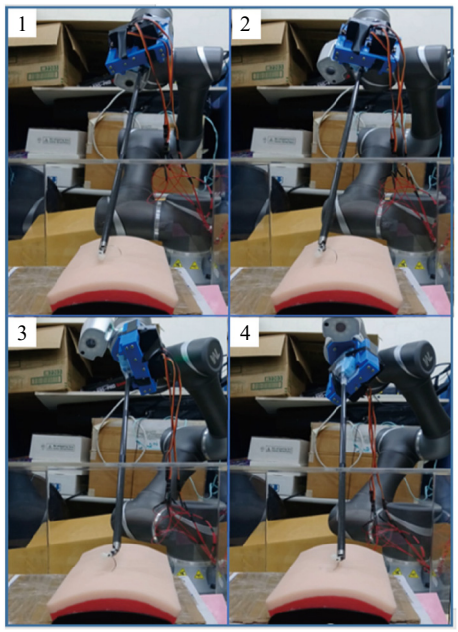

Fig. 19. Real suturing motion applied to the practice model (1)

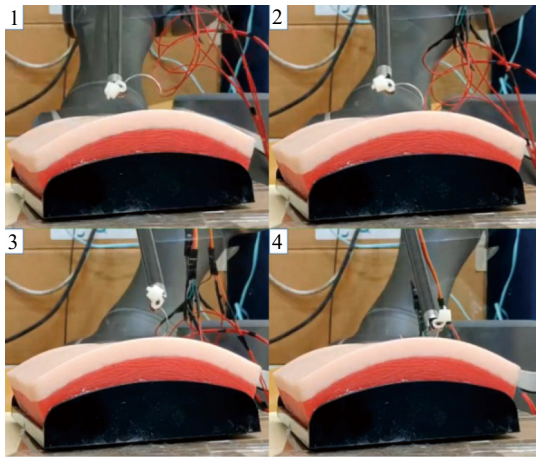

Fig. 20. Real suturing motion applied to the practice model (2)

controller; the commands are uploaded to the back-end robot arm and the Endowrist instrument to drive both at the same time. The simulation applied commands to simulate the same situation that occurred in the real-world system. The suturing practice model was used as the object of suturing. This is presented in Fig. 19 and Fig. 20.

VII. CONCLUSIONS

This study considered the environmental limitation of MIS and designed an MIS robot; the robotic arm's controlling system functions effectively and efficiently in the constrained conditions of RCM. Kinematic mathematical models were used to design the surgical motion of the robot and back-end robotic arm. The driving mechanism and the controlling

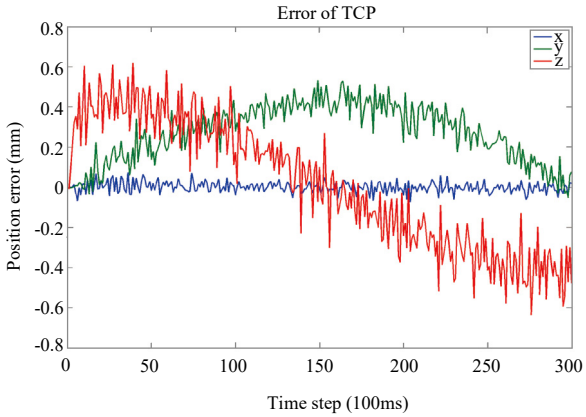

Fig. 21. Error of TCP during the real suturing process

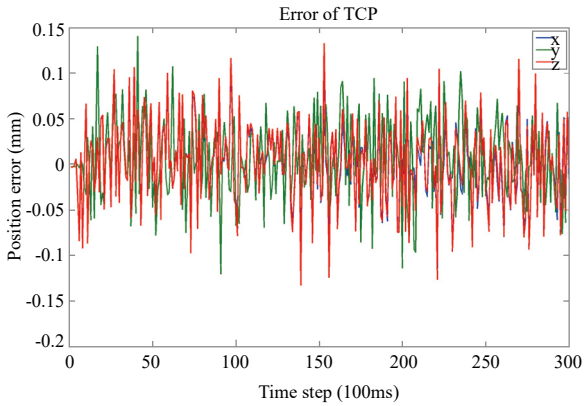

Fig. 22. RCM error during the real suturing process

program for the surgery clamp with two degrees of freedom were fixed at the end of the long tube. By combining the mechanism and the program, the MIS robot system with eight degrees of freedom was obtained. Based on the structure of the Endowrist instrument attached to the end of the robot arm, a robot arm control system with RCM was designed. To avoid lacerations in incisions, the RCM should be fixed. The inverse kinematics method was used to calculate the compensational angle of the integrated systems. The position and direction of the needle of the integrated systems can be controlled to realize delicate motion. The feasibility of applying this system to the MIS suturing process was proved through both simulation and experiment.

ACKNOWLEDGMENT

This work was supported in part by the Ministry of Science and Technology under Grant MOST 107-2221-E-002-177-MY3.

REFERENCES

Aghakhani, N., M. Geravand, N. Shahriari, M. Vendittelli, G. Oriolo(2013). Task control with remote center of motion constraint for minimally invasive robotic surgery. IEEE International Conference on Robotics and Automation, Karlsruhe, Germany, May 6-10.

Anderson, P. L., R. A. Lathrop, S. D. Herrell and R. J. Webster (2016). Comparing a mechanical analogue with the Da Vinci user interface: Suturing at challenging angles. IEEE Robotics and Automation Letters 1(2), 1060-1065.

Belli, G., P. Limongelli, C. Fantini, A. D'Agostino, L. Cioffi, A. Belli and G. Russo (2009). Laparoscopic and open treatment of hepatocellular carcinoma in patients with cirrhosis. British Journal of Surgery 96, 1041-1048.

Berducci, M., H. F. Fuchs, P. Omelanczuk, R. C. Broderick, C. R. Harnsberger, J. Langert, J. Nefa, P. Jaureguiberry, P. Gomez, L. Miranda, G. R. Jacobsen, B. J. Sandler, S. Horgan (2016). Phase II clinical experience and long-term follow-up using the next-generation single-incision platform FMX314. Surgical Endoscopy 30, 953-960.

Chen, C.-Y. (2017). Virtual Compliance Control Design For a Human Co-Working Endoscope Holding Robot, 1-81.

Chiang, S.-C. (2018). Kinematic Modeling and Camere Angle Control of an 8-DOF Endoscope Robot, 1-63.

Corke, P. (2011). Robotics, vision and control: fundamental algorithms in MATLAB. Springer,.

Craig, J. J. (2009). Introduction to robotics mechanics and control. 3rd Edition, Pearson Education International.

Deo, A. and I. Walker (1995). Overview of damped least-squares methods for inverse kinematics of robot manipulators. Journal of Intelligent & Robotic Systems 14(1), 43-68.

D'Ettorre, C., G. Dwyer, X. Du, F. Chadebecq, F. Vasconcelos, E. De Momi and D. Stoyanov (2018). Automated pick-up of suturing needles for robotic surgical assistance. Proceedings - IEEE International Conference on Robotics and Automation 2018, 1370-1377.

Fuchs, K. H. (2002). Minimally Invasive Surgery. Endoscopy 34, 154,159, 14.08.

Guthart, G. S. and J. K. Salisbury (2000). The Intuitive/sup TM/telesurgery system: overview and application," in Proceedings 2000 ICRA. Millennium Conference. IEEE International Conference on Robotics and Automation. Symposia Proceedings (Cat. No. 00CH37065), 618-621.

Hannaford, B., J. Rosen, D. W. Friedman, H. King, P. Roan, L. Cheng, D. Glozman, J. Ma, S. N. Kosari and L. White (2013). Raven-II: an open platform for surgical robotics research. IEEE Transactions on Biomedical Engineering 60(4), 954-959.

Horeman, T., E. J. Meijer, J. J. Harlaar, J. F. Lange, J. J. Van Den Dobbelsteen, and J. Dankelman (2013). Force sensing in surgical sutures. PLoS ONE, Article 8(12), Art no. e84466.

Jackson, R. and M. Cavus¸o˘glu (2013). Needle Path Planning for Autonomous Robotic Surgical Suturing. IEEE International Conference on Robotics and Automation, 1669-1675.

Kaneko, H., S. Takagi, Y. Otsuka, M. Tsuchiya, A. Tamura, T. Katagiri, T. Maeda and T. Shiba (2005). Laparoscopic liver resection of hepatocellular carcinoma. The American Journal of Surgery 189, 190-194.

Laurent, A., D. Cherqui, M. Lesurtel, F. Brunetti, C. Tayar, and P.-L. Fagniez (2003). Laparoscopic liver resection for subcapsular hepatocellular carcinoma complicating chronic liver disease. Arch Surg 138, 763-769.

Leonard, S., A. Shademan, Y. Kim, A. Krieger and P. C. W. Kim (2014). Smart Tissue Anastomosis Robot (STAR): Accuracy evaluation for supervisory suturing using near-infrared fluorescent markers. Proceedings - IEEE International Conference on Robotics and Automation , 1889-1894.

Leonard, S., K. L. Wu, Y. Kim, A. Krieger and P. C. W. Kim (2014). Smart tissue anastomosis robot (STAR): A vision-guided robotics system for laparoscopic suturing. IEEE Transactions on Biomedical Engineering 61(4), 1305-1317.

Li, Q., J. M. Hervé and P. Huang (2017). Type synthesis of a special family of remote center-of-motion parallel manipulators with fixed linear actuators for minimally invasive surgery. Journal of Mechanisms and Robotics 9(3), 031012.

Liu, T. and M. C. Cavusoglu (2016). Needle grasp and entry port selection for automatic execution of suturing tasks in robotic minimally invasive

surgery. IEEE Transactions on Automation Science and Engineering, Article 13(2), 552-563, Art no. 7384768.

Marinho, M. M., K. Harada and M. Mitsuishi (2017). Comparison of remote center-of-motion generation algorithms. IEEE/SICE International Symposium on System Integration, 668-673.

Matteotti, R. A., W. Stanley, R. A. Matteotti, W. Stanley (Eds.) (2011). Minimally Invasive Surgical Oncology. Springer-Verlag Berlin Heidelberg XXXIII, 546.

Patnaik, V.V.G., R. K. Singla and V. K. Bansal (2001). Surgical incisions—Their anatomical basis. Journal of the Anatomical Society of India 50(2), 170-178.

Rosen, J. and B. Hannaford (2006). Doc at a distance. IEEE spectrum 43(10), 34-39.

Sandoval, J., G. Poisson and P. Vieyres (2017). A new kinematic formulation of the RCM constraint for redundant Torque-Controlled robots. IEEE/RSJ International Conference on Intelligent Robots and Systems, 24–28.

Spong, M. W., S. Hutchinson and M. Vidyasagar (2006). Robot Modeling and Control 3. New York: Wiley.

Sun, L.-W., F. Van Meer, Y. Bailly and C. K. Yeung (2007). Design and development of a da vinci surgical system simulator. International Conference on Mechatronics and Automation, 2007: IEEE, pp. 1050-1055.

Tranchart, H., G. Di Giuro, P. Lainas, J. Roudie, H. Agostini, D. Franco, and I. Dagher (2010). Laparoscopic resection for hepatocellular carcinoma: a matched-pair comparative study. Surgical Endoscopy 24, 1170-1176.

Wampler, C. W. (1986). Manipulator inverse kinematic solutions based on vector formulations and damped least-squares methods. IEEE Transactions on Systems, Man and Cybernetics 16(1), 93-101.

Wang, W., W. Wang, W. Dong, H. Yu, Z. Yan and Z. Du (2015). Dimensional optimization of a minimally invasive surgical robot system based on NSGA-II algorithm. Advances in Mechanical Engineering 7.2, 2015.